Desalination and Water Treatment
www.deswater.com

doi:10.5004/dwt.2019.23645

145 (2019) 1–10
March

Measurement of critical tractive force of sponge carrier media in a moving bed biofilm reactor and the application of computational fluid dynamics/discrete element method model simulation

Bing Liu[a,b], Mitsuharu Terashima[b,*], Magnus So[c], Hidenari Yasui[b]

[a]*School of Municipal and Environmental Engineering, Shandong Jianzhu University*
[b]*Faculty of Environmental Engineering, The University of Kitakyushu, Japan, email: b-liu@kitakyu-u.ac.jp (B. Liu), m-terashima@kitakyu-u.ac.jp (M. Terashima), hidenari-yasui@kitakyu-u.ac.jp (H. Yasui)*
[c]*Faculty of Engineering, Kyushu University, Japan, email: magnus_so@chem-eng.kyushu-u.ac.jp (M. So)*

Received 9 June 2017; Accepted 24 December 2018

ABSTRACT

Moving bed biofilm reactors (MBBRs) are commonly used to remove organic pollutants and ammonia from wastewater for water reuse as secondary treatment. In MBBRs, small, free-floating media are introduced into aeration tanks to provide a large surface area onto which microorganisms such as ordinary heterotrophic organisms and ammonia oxidizing organisms, can attach. We measured the settling velocity and the critical tractive velocity of the sponge carrier media in an operating full-scale MBBR aeration tanks. Critical friction Reynolds number, Re_C* was strongly related to the particle Reynolds number, Re_p ($r = 0.944$, $p < 0.01$). Based on this, the critical parameters for distinct element method computational fluid dynamics (CFD-DEM) simulations were obtained. The simulation results were compared to the measured deposition in one of the MBBR aeration tanks. Based on the results of the physical model and CFD-DEM simulations, a modified configuration was proposed to reduce deposition.

Keywords: Critical tractive force; MBBR; Sponge carrier media; CFD-DEM; Wastewater

1. Introduction

Moving bed biofilm reactors (MBBRs) are aerobic biological wastewater treatment systems for water reuse in which microorganisms attached to moving carrier media oxidize organic pollutants and/or ammonia nitrogen [3]. MBBR systems enable a stable and high concentration of microorganisms to be maintained [4,5] in contrast to conventional activated sludge systems, and have almost no risk of blockage of carrier media unlike fixed bed biological systems (such as trickling filters and contact aeration processes). Although the up-flow anaerobic sludge blanket (UASB) reactors were developed for the effective domestic wastewater treatment [6–8], because of these advantages, MBBRs have become one of the most common biological wastewater treatment systems [9,10].

Cubic media made from polyurethane foam are commonly used in MBBRs, because of their high bacteria attachment ability, mobility, and low cost. However, media deposition can cause problems, such as shortening the hydraulic retention time (HRT) by reducing the active tank volume, and reducing the effective concentration of media. Therefore, minimum bottom velocity is needed to prevent media deposition on the tank bottom.

To examine deposition and solids transport phenomena in water, particles in a channel have been studied in many previous researches. Based on the concept that particles on the bottom surface start moving when the lifting force of the turbulence exceeds their weight, Einstein [11] introduced the concept of pick-up rate per unit time to develop a theory of solids transport. Moreover, Iwagaki [12], expanding the pioneering experimental work by Shields [13], introduced the theoretical relation between the friction Reynolds number and a dimensionless critical tractive force from

*Corresponding author.

the statistical equilibrium to summarize a large amount of experimental data. This relation was based on the concept that the particles start moving when the drag force exceeds the frictional resistance. To analyze the critical tractive force in an engineering context, Iwagaki's method is useful, and has been applied to the design of an open channel.

As for particles in a channel, the critical tractive force of bacteria-attached sponge carrier media in an operating MBBR can be summarized from the balance between drag and friction. However, bacteria-attached sponge carrier media in an operating MBBR differ from particles in a channel as follows. (1) The densities of sponge carrier media are close to that of water, and smaller than those of particles. (2) The grain density is almost constant, and can be obtained from its material properties, or be easily measured. However, the density of bacteria-attached sponge carrier media in an operating MBBR is difficult to measure, and is affected by the attachment of scale, bacteria, and bubbles. (3) Sponge carrier media have rough surfaces onto which bacteria attach. (4) Sponge carrier media are regular cubes; hence, the research results for grain in rivers cannot be directly applied to bacteria-attached sponge carrier media in an operating MBBR.

Terashima, Yasui and Takahashi [14] measured the bottom velocity required to prevent deposition of bacteria-attached sponge carrier media in five MBBR reactors. They found that the deposition position in the aeration tank corresponded to the low-velocity region calculated using computational fluid dynamics (CFD) simulation. However, they did not directly simulate the deposition of sponge carrier media. To simulate the particle movement in the fluid, the distinct element method (DEM) can be combined with CFD [15]. The reason for choosing the DEM approach is that the particle mixtures in MBBR systems are dense which makes Lagrangian solvers more accurate. A particle mixture is defined to be dense if the characteristic fluid response time for a particle is higher than the time between collisions [16]. CFD-DEM simulations have been used just to simulate the biofilm reaction in sponge carrier media particles in an MBBR reactor [17]. The two parameters of apparent density and friction coefficient are critical to estimate the deposition phenomena in the CFD-DEM simulation. But there are no critical studies about the measurement of these parameters.

The aim of this paper is to clarify the physical properties of the sponge carrier media and the tractive force to avoid deposition. Therefore we analyzed the relation between two dimensionless numbers, the particle Reynolds number and friction Reynolds number, in a physical model and obtained new critical parameters in CFD-DEM. Then, CFD-DEM simulations were conducted to predict the deposition. Subsequently, these simulations were used to propose a modified configuration of the MBBR tank.

2. Materials and methods

2.1. Terminal settling velocity and apparent density of cubic MBBR media

The settling of MBBR media in a liquid can be expressed by a motion Eq. (1). The force due to gravity, F_G and the drag force during settling, F_F were expressed by Eq. (2) and Eq. (3) respectively [18].

$$M\frac{du_f}{d_t} = F_G - F_F \tag{1}$$

$$F_G = g\rho\left(\frac{\sigma}{\rho}-1\right)\left(\frac{\pi d_s^3}{6}\right) \tag{2}$$

$$F_F = \frac{\rho C_D}{2}\left(\frac{\pi d_s}{4}\right)u_f^2 \tag{3}$$

When the media is settling at the terminal settling velocity, the terminal settling velocity, u_t is used in place of the settling velocity, u_f and the time rate of change of velocity (du/dt) is equal to zero. Then, combining Eqs. (1)–(3) yields Eq. (4), by which specific density difference ($\sigma/\rho - 1$) was calculated.

$$\left(\frac{\sigma}{\rho}-1\right) = \frac{3}{4}\frac{u_t^2}{gd_s}C_D \tag{4}$$

MBBR media are cubic; hence, the relation between d_s and d_c can be expressed as follows:

$$d_s = \left(\frac{6}{\pi}\right)^{\frac{1}{3}} d_c \tag{5}$$

The C_D for each cube can be expressed as shown in Eq. (6) [15].

$$C_D = \frac{24}{\mathrm{Re}_p}\left(1 + A\mathrm{Re}_p^B\right) + \frac{C}{1+\frac{D}{\mathrm{Re}_p}} \tag{6}$$

$$\mathrm{Re}_p = \frac{d_s u_t \rho}{\mu} \tag{7}$$

where A, B, C, D are non-dimensional constants and the values are $A = 0.2736$, $B = 0.5510$, $C = 1.406$, $D = 762.39$, respectively, by Haider and Levenspiel [15]. This C_D model was chosen in this study because it is most commonly used for nonspherical particles and has been cited in many papers even recently [19–24]. Because the specific density difference is defined by ($\sigma/\rho - 1$), the positive value of specific density difference means the density of particle is higher than that of water.

2.2. Critical tractive force

The horizontal forces applied to the media laying on the bottom of the tank are shown in Fig. 1. The magnitude of drag force (F_D) and the friction force (F_μ) are described in Eqs. (8) and (9), respectively.

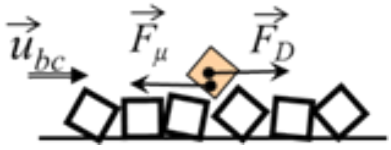

Fig. 1. Forces on a medium at the bottom of a tank.

$$F_D = \frac{\varepsilon_0 \rho C_D}{2}\left(\frac{\pi d_s}{4}\right)u_b^2 \tag{8}$$

$$F_\mu = \mu_s \rho\left(\frac{\sigma}{\rho}-1\right)g\left(\frac{\pi d_s^3}{6}\right) \tag{9}$$

The shielding coefficient, ε_0 expresses the effect that the particle is partly shielded from the flow by other particles at the bottom [2]. This shielding effect occurs only at the bottom of the tank and not for the settling particles. On the other hand tractive force was measured at the bottom in the presence of other particles. The drag force coefficient C_D can be calculated using Eq. (6). The forces are balanced when the media start depositing, as shown in Eq. (10).

$$F_D = F_\mu \tag{10}$$

Substituting Eqs. (8) and (9) into Eq. (10) gives Eq. (11) [2]. The velocity when the force is balanced and the media start depositing is defined as the critical velocity, u_{bc}, which is used instead u_b in Eq. (11).

$$\frac{u_{bc}^2}{\left(\frac{\sigma}{\rho}-1\right)gd_s} = \frac{4\mu_s}{3\varepsilon_0 C_D} \tag{11}$$

Combining Eqs. (4) and (11) yields Eq. (12).

$$u_{bc} = \sqrt{\frac{\mu_s}{\varepsilon_0}}u_t \tag{12}$$

The mean velocity (u_m) in the channel was measured in the experiment reported in Section 4.2. The velocity at the center height of the media was calculated from the vertical velocity distribution in the open channel. The vertical velocity distribution in the rough open channel can be described as shown in Eq. (13) [1,12].

$$\frac{u_z}{u^*} = 8.5 + 5.75\log_{10}\left(\frac{z}{k_s}\right) \tag{13}$$

The relation between u_m and u^* is shown in Eq. (14) [1,12].

$$\frac{u_m}{u^*} = 6.0 + 5.575\log_{10}\left(\frac{h}{k_s}\right) \tag{14}$$

For u_b at a particular height, the corresponding z_b is equal to $0.5 \times d_S$ [1]. The friction Reynolds number is defined in Eq. (15).

$$\mathrm{Re}^* = \frac{ds u_c^* \rho}{\mu} \tag{15}$$

The critical friction Reynolds number (Re_c^*) can be calculated from the critical friction velocity (u_c^*).

2.3. Sponge carrier media in operating MBBR tanks

The settling velocity and critical tractive forces for the bacteria-attached sponge carrier media were measured in operational MBBR tanks in five industrial wastewater treatment plants [14]. These MBBR aeration tanks were operated under conditions of pH around 7 and DO around 3–6 mg/L however these are changing due to the fluctuating inlet condition. Tank II–V were operated under volumetric loading rates between 1–5 kg/m^3 d and removal efficiency of BOD between 80–100%. The properties are shown in Table 1. The media were made of foam polyurethane cubes, with side lengths of 3 (Media ID, A) or 5 mm (Media ID, B–F). The specific surface area of sponge media in Tank I and II–V were 380 m^{-1} and 230 m^{-1} respectively. Sampled media A–E were kept in a refrigerator until the day prior to the measurements of their settling velocities and critical tractive forces. Media F was the same as media E, except that its settling velocity and critical tractive force were measured immediately after sampling. The protein content of each sample was measured [14] using the Bradford protein assay method [25]. For measurement of the attached solids, the sponge carrier media were washed thoroughly in distilled water to remove the attached solids, and the suspended solid (SS) in the liquid was measured. The amount of attached protein and solids was shown for each sponge carrier media in Table 1. The final settling velocities were measured using a transparent vertical cylinder (diameter: 200 mm; water depth: 300 mm) with lines marked at depths of 100 and 250 mm. The cylinder was filled with treated water from the MBBR systems. The sponges were released into the cylinder from just below the water surface. The final settling velocities were measured at the points when the sponges passed the two marked lines. Either 30 or 50 sponges were measured for each MBBR tank. These tests were dynamically conducted for a few seconds for one batch measurement.

2.4. Measurement of critical tractive force

The critical tractive force was measured [14] using an open-channel setup shown in Fig. 2. This consisted of an

Table 1
Bacteria-attached sponge carrier media

Media ID	Width (mm)	Tank ID	Wastewater source	Target material in wastewater	Protein in attached solid (mg L^{-1})	Attached solid (mg L^{-1})
A	3	I	Electrical	NH_4	10.7	–
B	5	II	Beverage	BOD	13.9	–
C	5	III	Chemical	BOD	6.4	–
D	5	IV	Beverage	BOD	7.5	–
E	5	V	Beverage	BOD	4.5	62.5
F	5	V	Beverage	BOD	–	–

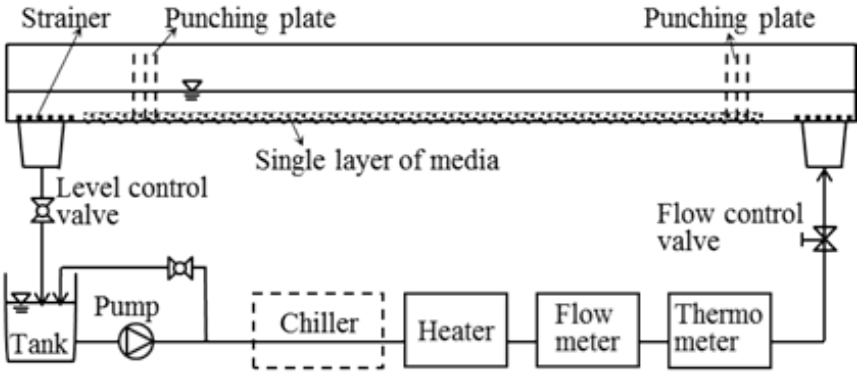

Fig. 2. Setup for critical tractive force measurements.

open channel (W: 100 mm, H: 100 mm), centrifugal pump, reserve tank, flow control valve, water-level control valve, flow meter, temperature meter, and a set of temperature controllers. The sponges were randomly attached on the bottom of the channel to simulate irregular deposition at the bottom of the tank. At the upper and lower stream ends of the channel, two sheets of perforated plates were installed to smoothen the flow. The same water used for the settling velocity measurements was recirculated by the pump. The temperature was manually controlled at 30.0 p/m 0.5°C by bar-type alcohol thermometer, chiller and heater. The pH values in the test samples were not measured. The hydraulic bottom height of the channel was defined as 0.5 d_s [1] above the media-attached surface. The water depth at the midpoint of the channel was set at 40 mm. Either 10 or 20 sponge carrier media were gently thrown into the upper channel. The number ratio of media reaching the end of the channel over the total number of media introduced into the channel was defined as the run-through ratio. This ratio was relative to the flow rate. These tests were dynamically conducted for a few seconds for one batch measurement.

2.5. Deposition of sponge carrier media in an operating MBBR tank

The deposition of sponge carrier media was measured in the same MBBR aeration tank in which sponge carrier media A were sampled [14]. This aeration tank was designated as Tank I (Table 2). Tank I contained a spiral-roll aeration system, wherein vertical-cylinder type aerators were installed widthwise along one side.

A video camera was encased in a concrete block with dimensions of 65 × 65 × 280 mm that had a window panel to enable video recording of carrier media in the liquid. The block was submersed lengthwise in a vertical manner with the leading end having a spherical shape for ease of submersion in case the carrier media deposited. Fig. 3 shows the insertion point of the video camera 500 mm off the wall opposite to the wall where the aerators were fixed in the tank. A video was recorded for 20 s at each depth. The lens was focused to record media immediately in front of the window. Beyond this the media was out of focus. When sponge carrier media came into focus and stopped, they were considered to have been deposited.

Table 2
Structure and operating conditions of Tank I

Item	Condition
Aeration tank volume, m^3	189
Tank depth, m	5.15
Tank width, m	3.9
Aeration intensity, m h^{-1}	64
Packing of media, %	19
Type of aerator	Cylindrical
Number of aerators	20

2.6. CFD-DEM coupling simulation

CFD-DEM coupling simulations were conducted to simulate the deposition of sponge carrier media in Tank I. RFLOW (R-flow Corporation Ltd) was used as a solver for CFD-DEM.

The water was modeled as a continuous fluid phase, and sponge media and air bubbles were modeled as dispersed phases with discrete particles undergoing collisions. The parameters for the CFD-DEM simulations are shown in Table 3. In the CFD solver, the fluid flow was calculated by solving the Reynolds-averaged Navier–Stokes (RANS) equations with the addition of the particle drag forces from the sponge media and air bubbles. Gidaspow drag correlation [26] was used to calculate the drag forces. The standard k-epsilon model was applied to model turbulence and is based on the assumption of isotropic turbulence. In order to accurately simulate turbulence near the walls, wall functions of Patankar and Spalding [27] was applied. The standard k-epsilon is said to be weak in describing flows with swirl and rotation. But because of the limitation of turbulence model of simulation software it was used in this study.

In the DEM solver, the velocity of each particle was calculated from the forces acting on it using Newton's laws of motion. The forces on the particles included buoyancy resulting from density differences relative to the surrounding water, fluid drag, and the contact and friction forces between nearby particles. The contact forces resulting from particle overlap were calculated using Hooke's law, with a spring constant of 1000 N m^{-1}. The bounce-back velocity was calculated with a restitution coefficient of 0.9. The fric-

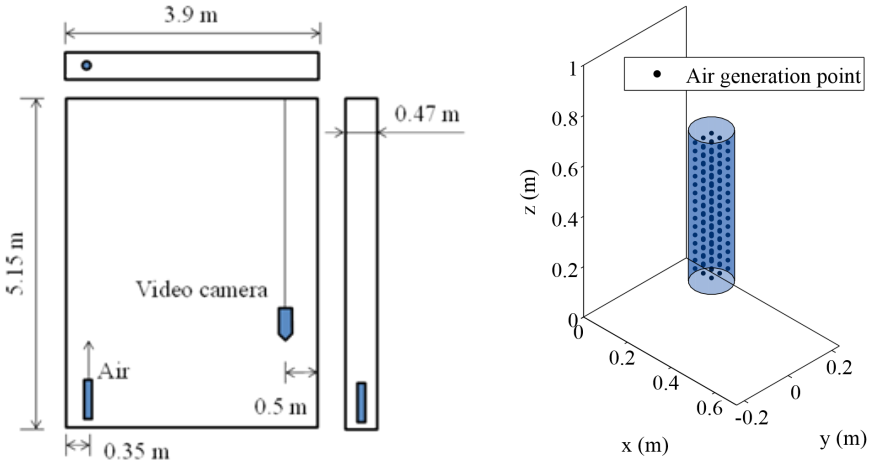

Fig. 3. Structure of aeration Tank I (left) and modelling of the air diffuser (right) for simulation.

Table 3
Parameters for the CFD-DEM simulation

Expression	Air bubbles	Sponges
Specific density difference, σ	–1.00	0.0069
Stokes diameter, m	0.00375	0.00375
DEM diameter ratio	8.33	16.67
Restitution coefficient	0.9	0.9
Spring constant, Nm^{-1}	1,000	1,000
Slide friction coefficient	0	1.3
Initial volume fraction	0	0.19
Initial number of particles	0	27,500

tion forces were calculated using the standard friction equation, with a measured friction coefficient of 1.3. The Stokes diameter, which is the equivalent diameter of a spherical particle with the same settling velocity, was set to 3.75 mm, based on a comparison of different drag correlations for cubic and spherical particles.

The tank had 20 aerators but considering the symmetry of configuration, only one aerator compartment was modeled for the simulation. The simulated geometry was a 470-mm-thick slice of a full-scale MBBR aeration Tank I (Fig. 3, left). The diffuser was positioned at the bottom-left. The diffuser was modeled as a 0.6-m-long hollow cylinder with a diameter of 0.15 m. Air particles were generated inside the cylinder (Fig. 3, right) with an overall aeration intensity of 64 m h^{-1}, in accordance with the corresponding experiment. The aeration intensity was defined as the air flow rate (m^3 h^{-1}) per tank area (m^2). A total of 27,500 sponge particles were initially distributed homogeneously with an average volume fraction of 19%. No-slip boundary conditions were applied to the side and bottom walls, and symmetry boundary conditions were applied in ±y directions. The water surface was modelled as a free slip surface under degassing conditions. This means when air particles go outside this boundary they would permanently exit the domain whereas sponge particles would be bounced back.

Fluidized sponge was defined as the sponge with a velocity higher than 0.02 m s^{-1}. The settling height from the bottom was defined as the level from the bottom to fluidized sponge.

The number of elements for the fluid flow was 27 thousand. The average and minimum orthogonality were 0.98 and 0.82, the average and maximum skewness were 0.0563 and 0.410 and the average and maximum aspect ratio were 4.33 and 12.6 respectively. The time step was 2.2 [ms] for the particles and 44 [ms] for the fluid phase. The total simulated time was 4415 [s] and 4509 [s] for current and baffle configuration respectively. SIMPLE algorithm with second order total variation diminishing (TVD) scheme was used. As an initial condition all velocities in the tank were zero and the sponges were distributed homogenously in the tank. A zero gradient boundary condition for velocity, turbulence kinetic energy and dissipation was applied at the symmetry planes and the water surface. Wall functions of Patankar and Spalding [27] were used which includes the logarithmic law of the wall. The current configuration simulation took 16.8 d and the baffle simulation 17 d with an Intel i7 CPU.

The CFD simulations of element number 240 thousands, 270 thousands and 300 thousands resulted in no difference in the velocity vertical distribution at the video camera observation point ($p << 0.01$ by Paired t-test), which indicated that the simulation results of element number at 270 thousands are independent to elements number, and the following simulations were conducted at this element number, mesh size.

The CFD simulations of element number 240 thousands, 270 thousands and 300 thousands resulted in no difference in the velocity vertical distribution at the video camera observation point ($p << 0.01$ by Paired t-test),which indicated that the simulation results of the element number at 270 thousands are independent to elements number, and the following simulations were conducted using this mesh. The settling height was also chosen as a target parameter in the mesh convergence test. Finer mesh and more particles did not alter the settling height. However, reducing the number of sponge particles from 27 thousands to 15 thousands resulted in a lower settling height.

3. Results and discussion

3.1. Terminal settling velocity of sponge carrier media

The distribution of particle Reynolds numbers (Re_p) from the measurements [14] of the terminal settling velocities of sponge carrier media is shown in Fig. 4. The measurements are summarized in Table 4. The median value was used as the representative value for each measurement. The relative standard deviations (RSDs) of the terminal settling velocities of the media in each tank ranged from 6.8 to 12.0, exhibiting low dispersion [28]. The calculated ($\sigma/\rho - 1$) values based on the measured terminal settling velocities are also shown in Table 4.

The ($\sigma/\rho - 1$) values of media were different; the largest value was approximately four times greater than the smallest. These differences were attributed to variations in the apparent density resulting from variations in amounts of attached bacteria, and inorganics and gases produced by bacterial activity. Bacterial activity was affected by organic load, inorganic concentrations in wastewater, dissolved oxygen concentration, substrate concentration, oxidation-reduction potential (ORP), and temperature [29,30]. In contrast, sponge carrier media in the same aeration tank did not exhibit variations in terminal settling velocity or Re_p, indicating that the moving media in the tank were well-mixed.

A negative correlation was found between "protein in attached solid" and "$\sigma/\rho - 1$" ($r = -0.76$, $p < 0.1$). The reasons were that much attached biofilm causes anoxic or anaerobic condition inside the sponge and generation of gases. Comparison of the same media after storage for a night in a refrigerator (E) and immediately after sampling (F) showed that immediate measurement resulted in approximately 10% higher terminal velocity and Re_p; furthermore, the RSD was reduced from 11.3 to 7.3. This was attributed to the lower concentrations of gases produced by bacteria activities present on media F.

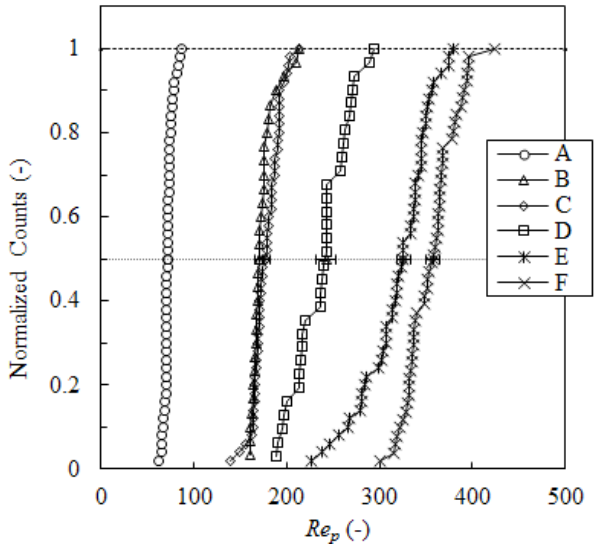

Fig. 4. Measured particle Reynolds numbers (Re_p) of MBBR media. The error bars indicate 95% confidence interval for median value.

Table 4
Measured apparent densities of media

Media	Re_p	RSD(%)	$\sigma/\rho - 1$
A	71.4	6.8	0.006946
B	171	7.5	0.006379
C	177	8.2	0.006759
D	241	12.0	0.011972
E	326	7.3	0.02158
F	358	11.3	0.02617

3.2. Critical tractive force of sponge carrier media

The relation between the tractive Reynolds number, Re^*, and normalized counts of run-through, η [14] are shown in Fig. 5. Small Re^* values corresponded with high levels of media deposition in the channel. At large Re^* values no media deposition occurred. At the critical Re^*, a rapid increase in η was observed. The measurement of the same media with different water depths (F and F′), provided a similar relation between Re^* and η. These results indicated that the run-through behavior of media could be accurately expressed using Re^*. The near-linear increase in η with Re^* was approximated by a straight line. The Re^* value at which the line intersects a horizontal line representing $\eta = 0.5$ was defined as the critical tractive Reynolds number, Re^*_c.

The relation between Re_p and Re^*_c is shown in Fig. 6. Based on the Pearson's Correlation Analysis, the critical friction Reynolds number, Re_C^* is strongly related to particle Reynolds number, Re_p ($r = 0.944$, $p < 0.01$). The calculation results for Eqs.(7)–(15), where $\mu_s = 1.3$, are also shown in Fig. 6. The experimental and calculated results were

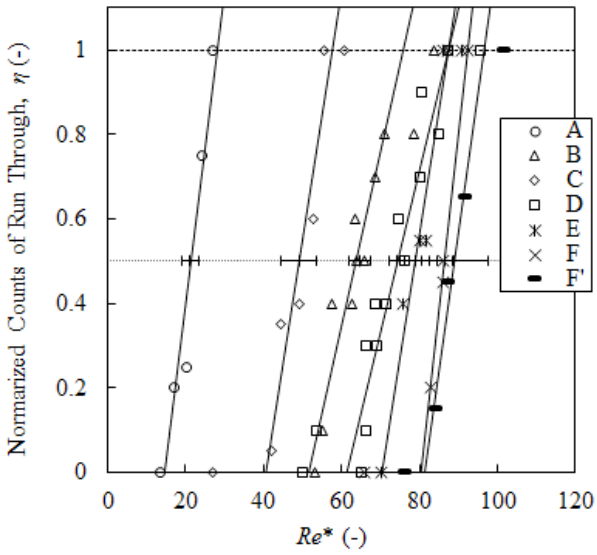

Fig. 5. The relation between the tractive Reynolds number, Re^*, and normalized counts of run-through, η. The error bars indicate 95% confidence interval for Re^*_c values, the critical tractive Reynolds number at which the line intersects a horizontal line representing $\eta = 0.5$.

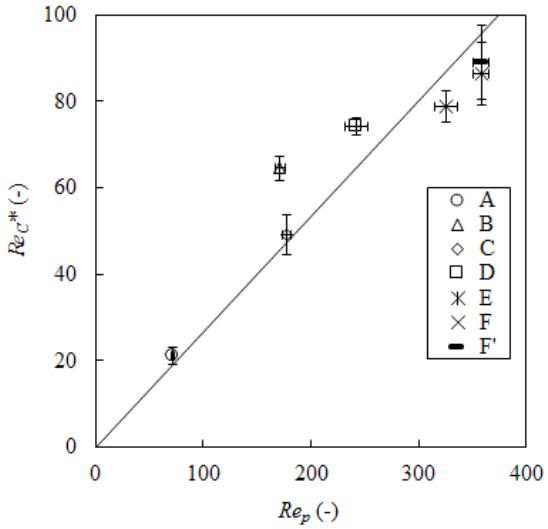

Fig. 6. Relation between particle Reynolds number (Re_p) and critical tractive Reynolds number (Re_c*). The error bars indicate 95% confidence interval.

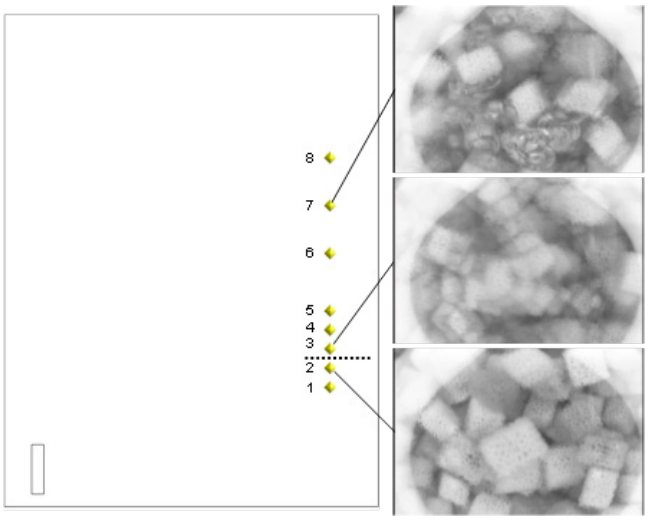

Fig. 7. Video camera observation of sponge media deposition in the full-scale FBBR aeration tank during operation [14]. The observation points were numbered. The dashed line indicates the observed deposition height.

best-fitted at μ_s = 1.3. Therefore, this value was found to be the most appropriate friction coefficient for sponge carrier media in the operating MBBR reactors. The friction coefficient for particles in a channel was reported to range from 0.933 to 1.118 [12]. Hence, the friction coefficient of sponge carrier media in the operating MBBR reactors was found to be larger than that of particles in a channel. This suggests that when differences in apparent density were taken into account, sponge carrier media required more tractive force than particles to avoid deposition.

The critical tractive force of the media should be measured to estimate the deposition of sponge carrier media in an MBBR tank. However, these measurements are very complicated. In contrast, the terminal settling velocity could be easily measured. The results of the present study revealed the relation between terminal settling velocity and critical tractive force, where μ_s = 1.3. This enabled the estimation of critical tractive force from the terminal settling velocity. On the other hand, for the practical implication, angle of repose, θ_R was calculated by the inverse tangent of the μ_s. From the result of this study, θ_R for sponge carrier media was estimated to be 52° and this was found to be the deposition angle when the sponge carrier media deposit.

3.3. Observation of media deposition in MBBR tank

Fig. 7 shows the observation results for deposition of sponge carrier media in MBBR Tank I [14]. Images obtained from video camera at representative heights are shown in Fig. 7. Near the bottom of the tank (at the observation points 1 and 2), the media in the frame did not move out of focus. Therefore, media were determined to be deposited at these heights. The observed deposition height (1.6 m from the bottom of the tank) is shown as a dashed line in Fig. 7. Above the deposition level (at the observation points 3, 4 and 5), the media were moving in and out of focus. Above the mid-point of the tank (at the observation points 6, 7 and 8), bubbles were observed in addition to the media.

3.4. CFD-DEM simulation of media deposition in MBBR tank

Fig. 8 shows the transient results for the media deposition region (dot-hatched area) and the velocity vectors. The settling height was defined by the region connected with the bottom and a volume fraction of sponges exceeding 30%. In the early stages ($0 < t \leq 120$ s), a deposition region formed at the bottom-left around the diffuser. The flow exhibited a clockwise circular pattern, with rising flow above the diffuser. From t = 300 s the settling region gradually moved to the right side of the tank away from the diffuser. After t = 1200 s, the results indicated a pseudo steady state with only minor fluctuations in the settling height.

3.5. Application of CFD-DEM simulation to a modified configuration

Additional simulations were conducted for a modified system containing a baffle (x = 1.95, $1 < z < 4.15$). The deposition region for the baffle configuration is shown at the bottom of Fig. 8 and to the right in Fig. 9. The height of the deposition region, the settling height, at the measurement location is shown in Fig. 10. After t = 1200 s, the results indicated a pseudo steady state with only minor fluctuations in the settling height at 1.79 ± 0.09 m (95% confidence interval). The distribution of the settling height at t = 2400 was significantly lower than for the initial configuration ($p < 0.01$), and the settled media was concentrated in the bottom corners of the reactor. In Fig. 10, the time series of the settling heights of the two configurations were compared. For the baffle configuration, the settling height was significantly lower (1.50 m difference and $p < 0.01$), and fluctuated (0.29 ± 0.22 m). As shown in Fig. 11, the fraction of fluidized media was significantly higher in the baffle configuration (74 ± 5%) in comparison to current configuration (16.3 ± 0.1%), ($p < 0.01$). Thus, the addition of a baffle improved the modeled fluidization performance.

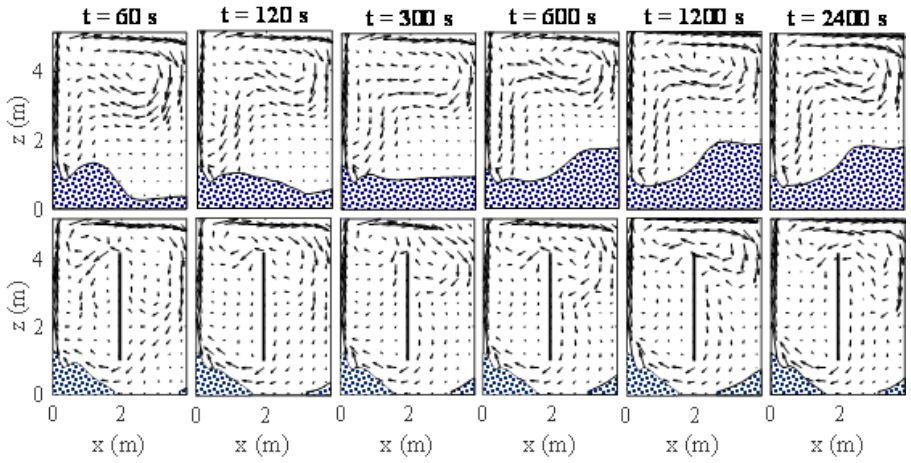

Fig. 8. Transient results of the velocity contours and carrier deposition regions.

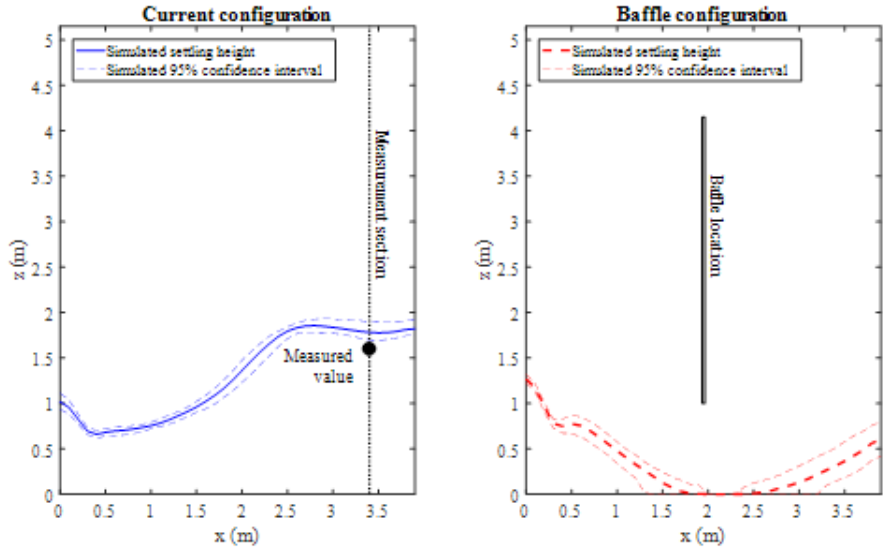

Fig. 9. Average settling heights at 1800 < t < 4600 s (thick lines) and 95% confidence intervals shown as thin lines.

3.6. Distribution of particles and velocity

Instantaneous positions of air and sponge particles at t = 2400 s are shown in Fig. 12, where the top figures (a–c) show the results for the initial configuration. In Fig. 12a, air particles occupied a region located 1–2 m below the water surface, and a thin column above the diffuser. The number of air particles fluctuated around 40,000, with an air volume fraction of 3.7 ± 0.3%. In Fig. 12b, sponge particles were present throughout the tank. The highest density was at the bottom right of the tank where they have settled. Contours of the water velocity are shown in Fig. 12c. The velocity was highest above the diffuser and near the water surface. At the bottom right, around the region of the settling zone, the velocity was close to zero. The water velocity contours obtained in the present study show similar patterns to previously published results of CFD simulations using a two-phase Eulerian approach for air and water (Terashima et al., 2012).

The corresponding results for the baffle configuration are shown in Figs. 12d–f. In Fig. 12d, air particles are

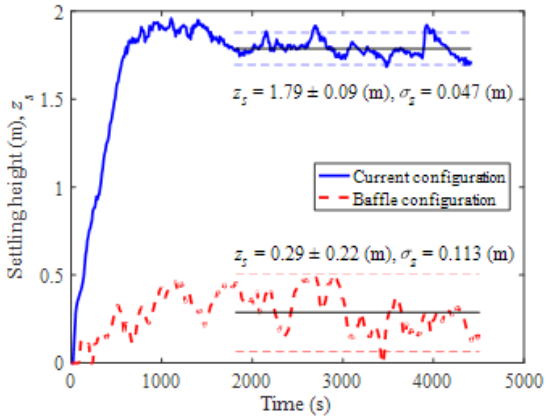

Fig. 10. Heights of settled sponges with time at section x = 3.4. Instantaneous values are shown as thick lines, and the confidence intervals (t > 1800 s) by thin lines.

distributed similarly to those in the initial configuration. However, the number of air particles and the air volume fraction were lower: 25,000 and 2.2%, respectively. In Fig. 12e, a larger proportion of sponges is shown to be fluidized, and to be distributed throughout the reactor. The reduced settling of sponge media can be partly described by the velocity contours shown in Fig. 12f. The area of the low-velocity region in the bottom right was substantially lower than that of the initial configuration.

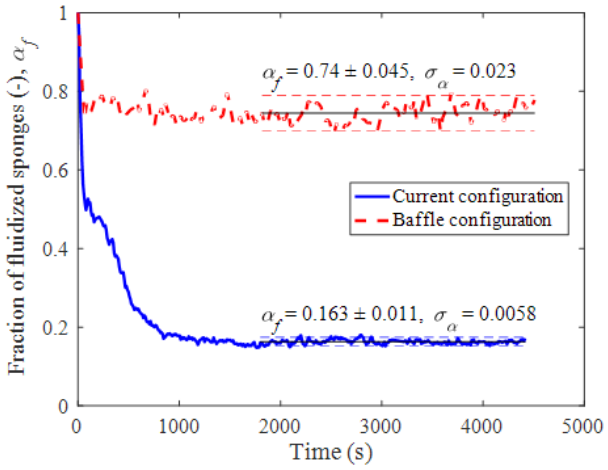

Fig. 11. Fraction of fluidized carrier media with time. Instantaneous values are shown as thick lines, and the confidence intervals (t >1800 s) by thin lines.

4. Conclusions

We measured the settling velocity and the critical tractive velocity for the sponge carrier media in operating full-scale MBBR aeration tanks. We obtained the friction coefficient of sponge carrier media, μ_s = 1.3, from the relation between two dimensionless numbers, the particle Reynolds number and friction Reynolds number. CFD-DEM was used for a dynamic simulation of media deposition in a spiral-roll aeration tank. CFD-DEM was demonstrated to accurately predict the height of accumulated deposited media by comparison with experimental results. The strength of the CFD works lies in the ability to simulate particle-particle interaction which is crucial in MBBR systems because of the dense particle flow regimes. CFD-DEM demonstrated that by adding a baffle in the tank, the fluidization performance was significantly improved and the fraction of deposited media was reduced by 71%.

Symbols

A	—	Non-dimensional parameter, = 0.2736, -
B	—	Non-dimensional parameter, = 0.5510, -
C	—	Non-dimensional parameter, = 1.406, -
D	—	Non-dimensional parameter, = 762.39, -
C_D	—	Drag coefficient, -
C_D,	—	Drag coefficient for bottom media, -
d_C	—	Side length of a cube, m
d_s	—	Diameter of a sphere with a volume equal to that of a cube with sides of length dc (m)
F_D	—	Drag force, N

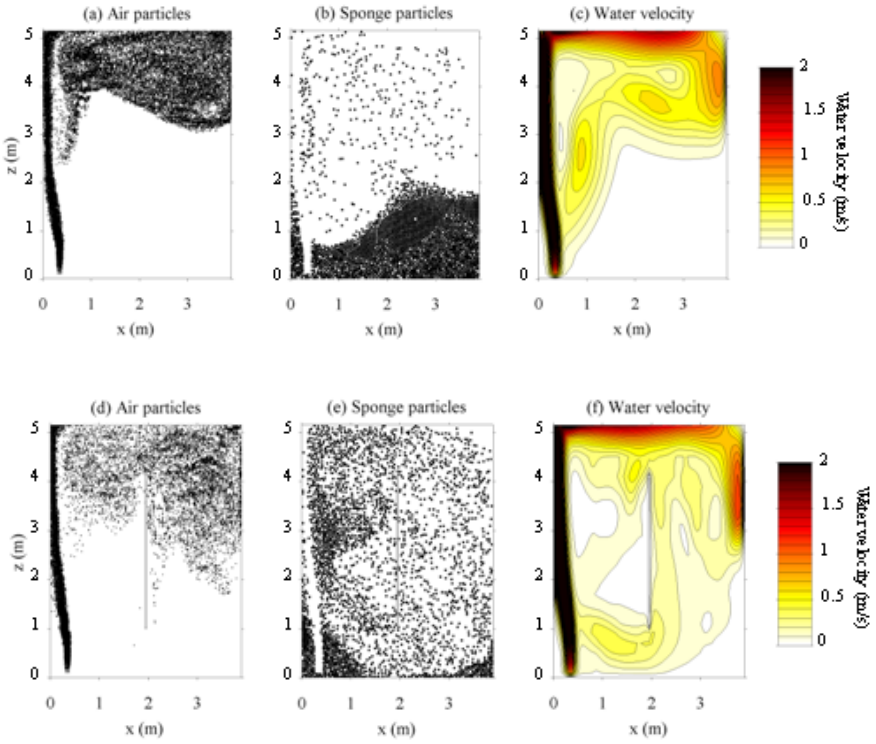

Fig. 12. Instantaneous air particle positions, sponge particle positions, and water velocity contours at t = 2400 s.

F_F — Drag force during settling, N
F_G — Force due to gravity, N
F_μ — Friction force, N
g — Gravitational acceleration, m s^{-2}
h — Water depth, m
k_s — Roughness of bottom, = d_s[1] , m
M — Particle mass, kg
Re^* — Friction Reynolds number, -
Re_c^* — Critical friction Reynolds number, -
Re_p — Particle Reynolds number, -
u^* — Friction velocity, m s^{-1}
u_b — Velocity of bottom media, m s^{-1}
u_{bc} — Critical velocity of the media, m s^{-1}
u_c^* — Critical friction velocity, m s^{-1}
u_f — Settling velocity, m s^{-1}
u_m — Mean velocity, m s^{-1}
u_t — Terminal settling velocity, m s^{-1}
u_z — Velocity of flow direction at a point z (m) above the bottom of the channel, m s^{-1}
z — Distance from bottom, m
ε_0 — Shielding coefficient, = 0.4 as determined by Iwagaki and Tsuchiya [2]
σ — Apparent density of particles, kg m^{-3}
$(\sigma/\rho - 1)$ — Specific density difference, -
μ — Liquid viscosity, Pa s
μ_s — Friction coefficient, -
ρ — Fluid density, kg m^{-3}

References

[1] S. Kusakabe, k. Dan, T. Yuki, Hydraulics (in Jpn), Corona Publishing Co., Ltd., Tokyo, 2002.
[2] Y. Iwagaki, Y. Tsuchiya, (II) On the critical tractive force for gravels on a granular bed in turbulent stream, Trans. Japan Soc. Civil Eng., 41 (1956) 22–38.
[3] H. Ødegaard, Innovations in wastewater treatment: the moving bed biofilm process, Water Sci. Technol., 53(9) (2006) 17–33.
[4] E. Rikmann, I. Zekker, T. Tenno, A. Saluste, T. Tenno, Inoculum-free start-up of biofilm- and sludge-based deammonification systems in pilot scale, Int. J. Environ. Sci. Technol., 15 (2018) 133–148.
[5] I. Zekker, E. Rikmann, K. Kroon, A. Mandel, J. Mihkelson, T. Tenno, T. Tenno, Ameliorating nitrite inhibition in a low-temperature nitritation–anammox MBBR using bacterial intermediate nitric oxide, Int. J. Environ. Sci. Technol., 14(11) (2017) 2343–2356.
[6] L. Daija, A. Selberg, E. Rikmann, I. Zekker, T. Tenno, T. Tenno, The influence of lower temperature, influent fluctuations and long retention time on the performance of an upflow mode laboratory-scale septic tank, Desal. Water Treat., 57(40) (2016) 18679–18687.
[7] T. Tenno, E. Rikmann, I. Zekker, T. Tenno, L. Daija, A. Mashirin, Modelling equilibrium distribution of carbonaceous ions and molecules in a heterogeneous system of $CaCO_3$-water-gas, Proc. Estonian Acad. Sci., 65(1) (2016) 68.
[8] E. Rikmann, I. Zekker, M. Tomingas, P. Vabamäe, K. Kroon, A. Saluste, T. Tenno, A. Menert, L. Loorits, S.S. dC Rubin, Comparison of sulfate-reducing and conventional Anammox upflow anaerobic sludge blanket reactors, J. Biosci. Bioeng., 118(4) (2014) 426–433.
[9] I. Zekker, E. Rikmann, A. Mandel, K. Kroon, A. Seiman, J. Mihkelson, T. Tenno, T. Tenno, Step-wise temperature decreasing cultivates a biofilm with high nitrogen removal rates at 9°C in short-term anammox biofilm tests, Environ. Technol., 37(15) (2016) 1933–1946.
[10] M. Raudkivi, I. Zekker, E. Rikmann, P. Vabamäe, K. Kroon, T. Tenno, Nitrite inhibition and limitation – the effect of nitrite spiking on anammox biofilm, suspended and granular biomass, Water Sci. Technol., 75(2) (2017) 313–321.
[11] H.A. Einstein, Formulas for the transportation of bed load, Trans. ASCE Paper, 2140 (1942) 561–597.
[12] Y. Iwagaki, (i) Hydrodynamical study on critical tractive force, Trans. Japan Soc. Civil Eng., 41 (1956) 1–21.
[13] F.A. Bombardelli, P.A. Moreno, Exchanges at the bed sediments-water column interface, In: C. Gualtieri, D.T. Mihailovic, Fluid Mechanics of Environmental Interfaces, CRC Press 2012, pp. 221–253.
[14] M. Terashima, H. Yasui, H. Takahashi, Critical tractive velocity and deposition of sponge media in fluidized-bed biofilm reactor (in Jpn), J. Japan Bio. Soc. Water Waste, 48(2) (2012) 45–53.
[15] Y. Tsuji, T. Kawaguchi, T. Tanaka, Discrete particle simulation of two-dimensional fluidized bed, Powder Technol., 77(1) (1993) 79–87.
[16] C.T. Crowe, J.D. Schwarzkopf, M. Sommerfeld, Y. Tsuji, Multiphase Flows with Droplets and Particles, CRC press, 2011.
[17] M. So, D. Naka, R. Goel, H. Yasui, Model development of a sponge carrier process using CFD-DEM with permeable particles, J. Water Environ. Technol., 10(2) (2012) 193–204.
[18] G.M. Fair, J.C. Geyer, D.A. Okun, Water and Wastewater Engineering, Water Purification and Wastewater Treatment and Disposal, John Wiley and Sons, Inc., New York, 1968.
[19] Z. Abbasi, A. Molaei Dehkordi, F. Abbasi, Numerical investigation of effects of uniform magnetic field on heat transfer around a sphere, Int. J. Heat Mass Transfer, 114 (2017) 703–714.
[20] V. Parisien, D. Pjontek, C.A. McKnight, J. Wiens, A. Macchi, Impact of catalyst density distribution on the fluid dynamics of an ebullated bed operating at high gas holdup conditions, Chem. Eng. Sci., 170 (2017) 491–500.
[21] R. Naveh, N.M. Tripathi, H. Kalman, Experimental pressure drop analysis for horizontal dilute phase particle-fluid flows, Powder Technol., 321 (2017) 355–368.
[22] A.A. Bhuiyan, A.S. Blicblau, J. Naser, Co-firing of biomass and slagging in industrial furnace: A review on modelling approach, J. Energy Inst., 90(6) (2017) 838–854.
[23] N. Paul, S. Biggs, J. Shiels, R.B. Hammond, M. Edmondson, L. Maxwell, D. Harbottle, T.N. Hunter, Influence of shape and surface charge on the sedimentation of spheroidal, cubic and rectangular cuboid particles, Powder Technol., 322(Supplement C) (2017) 75–83.
[24] S. Leguizamón, E. Jahanbakhsh, A. Maertens, S. Alimirzazadeh, F. Avellan, A multiscale model for sediment impact erosion simulation using the finite volume particle method, Wear, 392–393(Supplement C) (2017) 202–212.
[25] M.M. Bradford, A rapid and sensitive method for the quantitation of microgram quantities of protein utilizing the principle of protein-dye binding, Anal. Biochem., 72(1) (1976) 248–254.
[26] D. Gidaspow, Multiphase flow and fluidization: continuum and kinetic theory descriptions, Academic Press, California, 1994.
[27] S.V. Patankar, D.B. Spalding, Heat and Mass Transfer in Boundary Layers. 2nd ed., TBS The Book Service Ltd., 1970.
[28] A. Shinjo, Principles of Biostatistics (in Japanese), Asakura Publishing Co., Ltd., Tokyo, 2010.
[29] M. So, M. Terashima, R. Goel, H. Yasui, Modelling the bio-clogging of multispecies biofilms in sponge carrier media, J. Water Environ. Technol., 13(3) (2015) 263–278.
[30] M. So, D. Naka, R. Goel, M. Terashima, H. Yasui, Modelling clogging and biofilm detachment in sponge carrier media, Water Sci. Technol., 69(6) (2014) 1298–1303.